

Targeting HIF1 α /miR-22/CDK8/KAT5 feedback loop inhibits hepatocellular carcinoma development

Wei Huang¹, Yanqiu Li², Xiaojing Jia³, Chao Qu¹, Zhen Zhang⁴, Ruixin He⁵, Lizhe Wang⁶, Fengming Ni⁷, Donghe Su¹, He Huang^{8,9*}, Yaqin Qu^{1*}

¹.Department of Radiation Oncology, The First Hospital of Jilin University, Changchun, China

².Department of Radiation Oncology, Jilin Provincial Cancer Hospital, Changchun, China

³.Department of Radiation Oncology, The Second Hospital of Jilin University, Changchun, China

⁴.Department of General Surgery, the first affiliated hospital of Anhui medical university, Hefei, Anhui, China

⁵.Department of Clinical Medicine, West China Center of Medical Sciences, Chengdu, Sichuan.

⁶.Department of Pediatric oncology, The First Hospital of Jilin University, Changchun, China

⁷.Gastroenterology department, The First Hospital of Jilin University, Changchun, China

⁸.Department of Histology and Embryology, Xiang Ya School of Medicine, Central South University, Changsha, 410078 Hunan, The People's Republic of China

⁹.Cancer Laboratory, Second Affiliated Hospital of Xinjiang Medical University, Urumqi, 830063, China

Correspondence to : He Huang and Yaqin Qu

ABSTRACT

The glucose metabolism reprogramming is a hallmark of liver cancer. Although miR-22 has been reported to function as a tumor repressor in HCC, its role in aerobic glycolysis has not explicitly been explored. In this study, we supposed that miR-22 might be involved in the glucose metabolism reprogramming in hepatocellular carcinoma (HCC). We showed that knockdown of miR-22 caused a increase in generation of intracellular glucose and lactate, as well as a decrease in the oxygen consumption rate (OCR), which promotes metabolic switch from oxidative phosphorylation to aerobic glycolysis. Downregulation of miR-22-triggered glucose metabolism reprogramming promoted the growth of HCC *in vivo*. Mechanistically, miR-22 decreased the activity of hypoxia-inducible factor 1 α (HIF1 α) protein through directly targeting CDK8 and KAT5, forming a negative feedback loop of HIF1 α /miR-22/CDK8/KAT5/HIF1 α . Interestingly, we also indicated that HBx inhibited the miR-22 but elevated CDK8/KAT5 expression in HCC cells. Thus, these findings reveal a previously unappreciated function of miR-22 in HCC cell glycolysis and collectively highlight that miR-22 inhibits glucose metabolism reprogramming through suppressing CDK8/KAT5/HIF1 α axis, which may be considered as one of the powerful effective therapeutics for HCC patients.

Date of Submission: 20-07-2017

Date of acceptance: 05-09-2017

I. Introduction

Hepatocellular carcinoma (HCC) is the third leading cause of cancer-related death around the world (1). Understanding its molecular pathogenesis is pivotal to managing this disease. As both direct and indirect consequence of the mutations in oncogenes, such as c-Myc and hypoxia-inducible factor α (HIF1 α), HCC progression relies on cellular metabolic reprogramming, especially aerobic glycolysis, which is termed the “Warburg effect” (2,3). However, the underlying mechanisms are still poorly understood.

MicroRNAs (miRNAs) are small 19–24 bp long endogenous noncoding RNA molecules with high post-transcriptional regulatory activity, which functions primarily to down-regulate gene expression in all metazoan eukaryotes (4). MiRNA is emerging as an important driver in several aspects of hepatocarcinogenesis (5). Accumulating evidence reveals that miRNAs can regulate multiple targets and one gene can be under the regulation of several miRNAs (6). Recent evidences suggested that miR-22 is silenced in HCC and functions as a very important tumor suppressor (7, 8). However, it remains poorly understood whether miR-22 is involved in the glucose metabolism reprogramming in HCC.

In this study, we not only were interested in the effect of miR-22 on the glucose metabolism reprogramming in HCC, but also sought to gain insight into the regulatory mechanisms of miR-22 in HCC. Our data show that miR-22 inhibits the glycolysis in HCC cells, which is involved in the negative feedback loop: HIF1 α /miR-22/KAT5/CDK8/HIF1 α . We also show that aberrant expression of miR-22/CDK8/KAT5 axis is associated with HBV-related hepatocarcinogenesis. Our findings provide new insights into the mechanism by which miR-22

suppresses the glucose metabolism reprogramming in HCC, implicating high therapeutic potential of this regulatory loop for the management of HCC.

II. Results

Downregulation of miR-22 promotes glycolysis in HCC cells.

To determine whether miR-22 downregulation switches oxidative phosphorylation to glycolysis in HCC cells, we generated Huh7 cells with miR-22 knocked down. It was found that miR-22 knockdown increased lactate production and glucose uptake measured by ^3H -labeled deoxyglucose (Figure 1A and B). In addition, miR-22 knockdown reduced oxygen consumption in Huh7 cells (Figure 1C). The cells with miR-22 knockdown also exhibited lower levels of the extracellular acidification rate (ECAR) after treatment with glucose or oligomycin compared with the negative control (Figure 1D). The glycolysis under basal conditions, the glycolytic capacity and the glycolytic reserve were both enhanced when miR-22 was decreased in Huh7 cells (Figure 1E).

We also investigated lactate production, glucose uptake, and oxygen consumption in HCC cells overexpressing miR-22. Glucose uptake and lactate production were downregulated in miR-22-overexpressing HCC cells compared to control cells (Figure 1F and G). Overexpressing miR-22 also decreased oxygen consumption in these cells (Figure 1H). Furthermore, oxidative phosphorylation, as reflected by the maximum respiration capacity, increased in HCC cells overexpressing miR-22.

Taken together, these data demonstrate that miR-22 downregulation is critical for switching energy metabolism from oxidative phosphorylation to glycolysis in Huh7 cells.

MiR-22 inhibits glucose metabolism in HCC cells by targeting KAT5 and CDK8

To determine the action mechanism of miR-22, it is important to identify a mRNA target of miR-22 that might mediate the role of miR-22 in HCC cell glycolysis. The target prediction programs miRBase and TargetScan were utilized to predict the possible miR-22 targets. KAT5 and CDK8 attracted our attention because of two following reasons: 1, their 3'-UTRs contain a putative target sequence for miR-22 (Figure 2A); KAT5 and CDK8 have been reported to be closely involved in cancer glycolysis (9). To confirm that KAT5 and CDK8 were directly inhibited by miR-22, a dual-luciferase reporter system was used. We found that miR-22, not miR-1, significantly reduced firefly luciferase in the KAT5 or CDK8 3'UTR luciferase reporter assay (Figure 2A and B). When the several nucleotides in the KAT5 and CDK8 3'UTR that were predicted to associate with miR-22 were mutated (Figure 2A and B, indicated in red), miR-22 lost the ability to inhibit firefly luciferase expression. These data suggest that miR-22 is involved in KAT5 and CDK8 downregulation.

To confirm that miR-22 regulates the protein expression of KAT5 and CDK8, knockdown or overexpression of miR-22 was used. It was found that knockdown of miR-22 significantly increased the levels of KAT5 and CDK8 whereas miR-22 overexpression had the opposite effects in HCC cells (Figure 2C).

We next examined whether miR-22 exerts its inhibitory effects on glucose metabolism by targeting KAT5 and CDK8. We firstly analyzed glycolysis-related enzymes by quantitative PCR in miR-22-overexpressing HCC cells. MiR-22 overexpression decreased the expression of glycolysis-related enzymes, including PFKM, HK2, and GLUT1, while rescue expression of KAT5 or

CDK8 blocked the miR-22-induced downregulation of these molecules (Figure 2D). Furthermore, glucose uptake, lactate production, and oxygen consumption in HCC cells overexpressing miR-22 were rescued by CDK8 or KAT5 coexpression (Figure 2E and F). These results indicate that overexpression of KAT5 or CDK8 reverts the inhibitory effect of miR-22 on glycolysis in HCC cells, supporting the idea that targeting KAT5 or CDK8 is an important mechanism of miR-22-mediated suppression of glycolysis in HCC cells..

The miR-22-KAT5/CDK8 axis significantly inhibits tumorigenesis and migration of HCC cells.

We next asked whether the miR-22-KAT5/CDK8 axis is important in regulating tumorigenesis of HCC cells. As expected, transfection of miR-22 mimics in Huh7 cells strongly reduced cell proliferation (Figure 3A), cell survival (Figure 3B), transwell cell migration (Figure 3C), and colony formation (Figure 3D) as well as the rate of xenografted tumor growth in nude mice (Figure 3E and F). Conversely, inhibition of miR-22 function by anti-miR-22 in Huh7 cells markedly increased cell proliferation and migration in cultured cells and tumor growth in nude mice (data not shown), indicating that miR-22 negatively regulates HCC tumorigenesis and metastasis. We next examined whether miR-22 exerts its tumor-suppressive effects in HCC cells by targeting KAT5 and CDK8. Overexpression of CDK8 or KAT5 strongly reversed the roles of miR-22 overexpression in Huh7 cells (Figure 3A,B , C and D). RNAi knockdown of KAT5 and CDK8 reproduced the phenotype observed with miR-22 silencing in Huh7 cells (data not shown). Importantly, co-transfection of miR-22-resistant KAT5 and CDK8 in miR-22-transfected Huh7 cells strongly overrode the effects of miR-22 on HCC tumorigenesis *in vivo* (Figure 3E and F). Collectively, these

results indicate that the miR-22-KAT5/CDK8 axis significantly inhibits tumorigenesis of HCC cells.

MiR-22 does not decrease the levels of HIF-1 α mRNA and protein, but inhibits HIF-1 α transcriptional activity in HCC cells

Since both CDK8 and KAT5 are two necessary co-activators for hypoxia-induced factor-1 α (HIF-1 α), a very important glycolysis mediator (9, 10), we next investigated the inhibitory effect of miR-22 on HIF-1 α . To this end, we firstly measured the HIF-1 α mRNA and protein levels after miR-22 treatment of HCC cells. We found that miR-22 treatment does not significantly change the HIF-1 α mRNA and protein levels (Figure 4A and B).

To determine whether miR-22 functionally suppresses HIF-1 α transcriptional activity, HIF-1 α responsive promoter activity (HRE-luciferase) or vascular endothelial growth factor (VEGF)-luciferase was measured. In this case, miR-22 dramatically down-regulated HIF-1 α promoter activity (Figure 4C) and its target genes involved in glycolytic metabolism: carbonic anhydrase 9 (*CA-IX*), pyruvate dehydrogenase kinase 1 (*PDK1*), glucose transporter 1 (*GLUT1*), and lactate dehydrogenase A (*LDHA*) under hypoxia in HCC cells (Figure 4D). Because HIF-1 α stimulates cancer cell motility and invasiveness under hypoxia (11), the inhibitory effect of miR-22 on cell migration increased by hypoxia was tested. Consequently, it was found that miR-22 strongly attenuated cell migration under hypoxia in HCC cells (Figure 4E). These results demonstrated that miR-22 suppressed cancer cell motility by inhibiting HIF-1 α target gene expression associated with cancer metastasis. Together, miR-22 does not decrease the levels of HIF-1 α mRNA and protein, but inhibits HIF-1 α transcriptional activity.

MiR-22 expression is transcriptionally inhibited

by HIF-1 α

Since hypoxia is a hallmark of cancer and miRNAs can be aberrantly expressed during stress conditions such as hypoxia (12, 13), we further explored whether the decreased expression of miR-22 in HCC cells is regulated by HIF-1 α or hypoxia. As shown in Figure 5A and B, after treatment with hypoxia or CoCl₂, the expression of HIF-1 α protein was increased, whereas the expression of miR-22 was decreased.

To further clarify whether miR-22 is regulated by HIF-1 α , HIF-1 α expression was manipulated to evaluate its effects on miR-22 expression. Silencing HIF-1 α upregulated miR-22 expression and impaired the CoCl₂-induced suppression of miR-22 (Figure 5C). In contrast, the overexpression of HIF-1 α significantly reduced miR-22 expression (Figure 5D).

To study the transcriptional regulation of miR-22, we retrieved mouse miR-22 promoter sequence from genomic sequence of *mir22hg* gene, based on homologous alignment to recently published human miR-22 promoter sequence (14). As shown in Figure 8E, the miR-22 proximal promoter region contains two HRE binding sites for HIF-1 α , suggesting that HIF-1 α transcriptionally regulates the expression of miR-22. ChIP assays revealed that the two HRE sites of the pre-miR-22 were occupied by HIF-1 α and that this binding was enhanced during hypoxia (Figure 5F). To further confirm whether the binding of HIF-1 α to the miR-22 promoter is functional, a luciferase reporter plasmid containing the miR-22 promoter was transfected into Huh7 cells. CoCl₂ significantly decreased the luciferase activity in Huh7 cells, whereas knockdown of HIF-1 α increased luciferase activity (Figure 5G). Taken together, these data suggest that miR-22 is transcriptionally inhibited by HIF-1 α during hypoxia.

HBx is critical in HBV inhibiting miR-22 expression in HCC cells

Given that HBV is widely accepted to be a main cause of HCC and HBx plays an important role in the progression of HBV-associated HCC (15), we next investigated the effect of HBV on miR-22 expression using HepG2 cells and HepG2.2.15 cells which constitutively replicate HBV relative to HepG2 cells. It was found that the miR-22 level in HepG2.2.15 cells was dramatically lower compared to HepG2 cells (Figure 6A), and that the level of miR-22 in HepG2 cells transiently transfected with HBV1.3 vector was also lower than that of corresponding control (Figure 6B).

After human HepG2 cells were transfected with HBs, HBc, HBp and HBx vector, respectively, HBx was the only protein encoded by HBV that inhibited miR-22 expression (Figure 6C). To further investigate the regulatory mechanisms of HBx and HBV on miR-22, we analyzed the effects of the HBx and HBV on the activity of miR-22 promoter in the HepG2 cells transfected with HBV1.3 by using luciferase reporter assay. The results showed that the promoter activity of miR-22 was significantly lower in HepG2-HBV cells or HepG2-HBx cells compared with the control group (Figure 6D), suggesting that both HBV and HBx downregulate the expression of miR-22 through inhibiting its promoter activity.

HBx is also important in HBV-induced CDK8 and KAT5 protein expression

Western blot analysis revealed increased CDK8 and KAT5 expression in HepG2.2.15 compared to HepG2 cells (Figure 7A). Moreover, HBx enhanced CDK8 and KAT5 expression more remarkably compared to HBs-, HBc-, HBp-transfected HepG2 cells or negative control (Figure 7B). With HBx silencing in HepG2.2.15 cells, the levels of CDK8 and KAT5 protein were

significantly downregulated (Figure 7C). All these strongly supported that HBx is the vital protein encoded by HBV that promotes the expression of CDK8 and KAT5 proteins.

The expression of miR-22, CDK8, and KAT5 is correlated in human HCC specimens

To test whether our above findings in HCC cells are clinically relevant, we examined the miR-22 levels as well as the levels of CDK8, and KAT5 mRNAs in 60 human HCC primary tumor and paired adjacent normal tissue specimens. qRT-PCR showed that miR-22 was significantly down-regulated in HCC tumors compared to normal tissues (Figure 8A), while the levels of CDK8 and KAT5 were significantly upregulated (Figure 8B and C). Importantly, we observed significantly lower miR-22 expression and significantly greater CDK8 and KAT5 expression in HCC tumors (Figure 8D). We found a significant inverse correlation between miR-22 and *CDK8* mRNA levels (Pearson's $R = -0.512$, $P < 0.05$; Figure 8E), or *KAT8* mRNA levels in tumor specimens ($R = -0.432$, $P < 0.05$; Figure 9F). Collectively, these results strongly suggest that the miR-22-CDK8/KAT5 regulatory axis that we have discovered is clinically relevant in HCC (Figure 8G).

Figure Legends

Figure 1 Downregulation of miR-22 promotes glycolysis in HCC cells. (A) Analysis of lactate production and glucose uptake (B) in Huh7 depleted of miR-22. Lactate production was measured at indicated time points. (C) Basal oxygen consumption, oxidative phosphorylation, and maximum respiration capacity of Huh7 cells after miR-22 knockdown. The histogram displays the basal level of oxygen consumption. (D and E)

ECAR was measured by the Glycolysis Stress test in Huh7 cell lines after the cells were treated with anti-NC or anti-miR-22, respectively. The glycolysis under basal conditions, the glycolytic

capacity and the glycolytic reserve were analyzed according to the methods. (F, G and H) The effects of miR-22 overexpression on glucose uptake, lactate production and oxygen consumption rate.

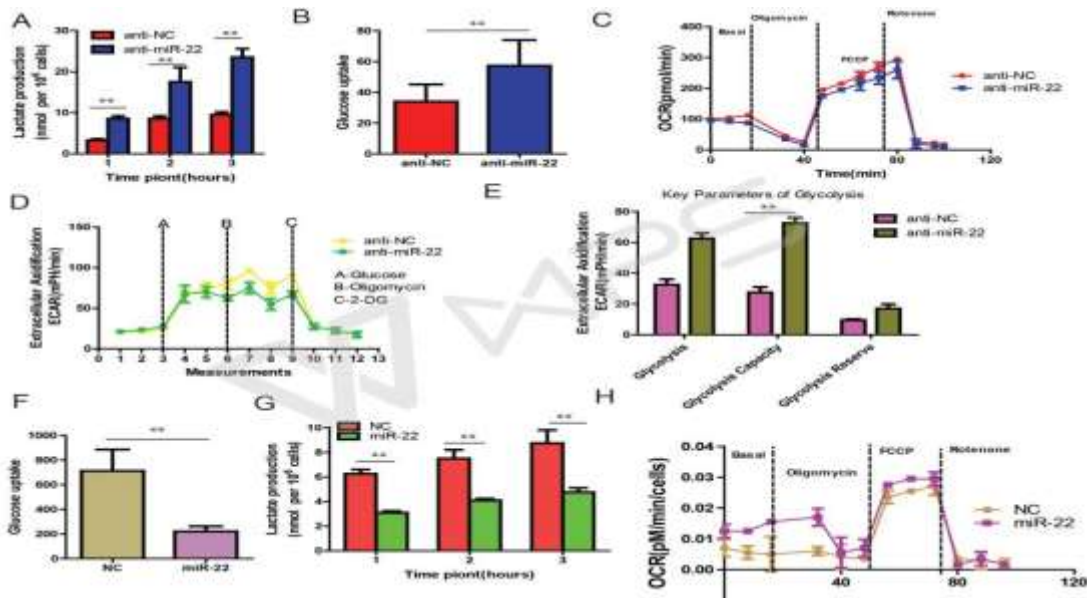


Figure 2 MiR-22 inhibits glucose metabolism in HCC cells by targeting KAT5 and CDK8

(A and B) miR-22, but not miR-1, regulates luciferase activity in wild-type or mutant KAT5 and CDK8 3' UTR groups. The nucleotides indicated in red for the KAT5 and CDK8 seed sequence were mutated to complementary nucleotides. (C) Knockdown or overexpression of miR-22 regulates KAT5 and CDK8 protein expression. (D) Effects of miR-22 overexpression on aerobic glycolysis. The mRNA level of Glut1, HK2, and PFKM in the HCC cells overexpressing miR-22 or KAT5 or CDK8 or as indicated. (E) The rate of lactate production and glucose uptake analyzed in HCC cells as indicated. (F) The diagram shows the effect of miR-22 or KAT5 or CDK8 overexpression on basal oxygen consumption, oxidative phosphorylation, and maximum respiration capacity.

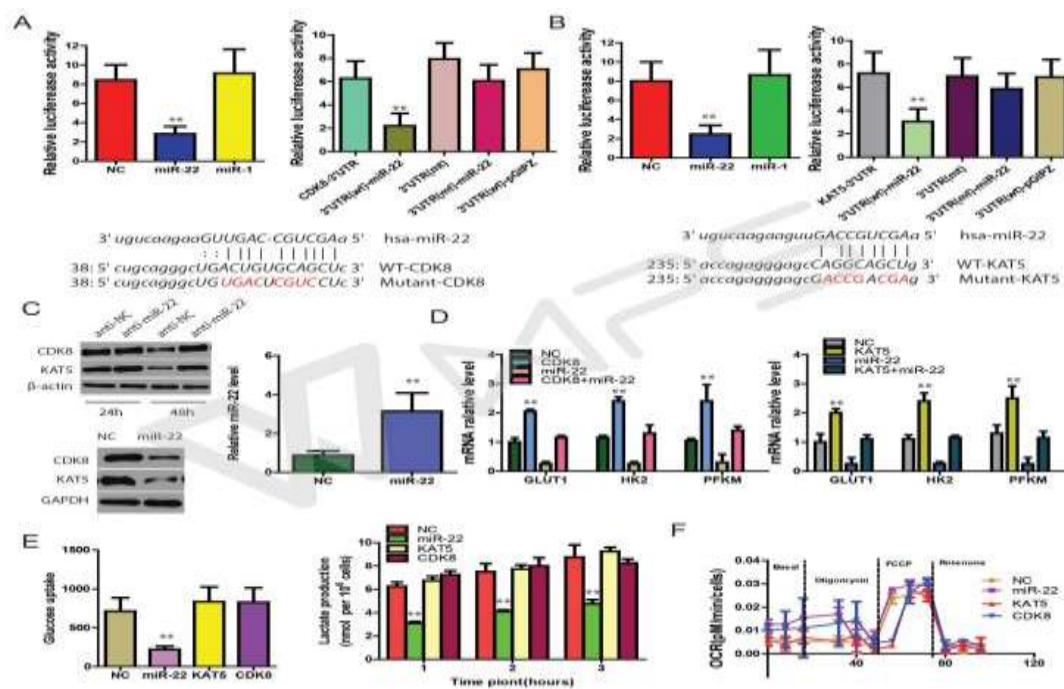


Figure 3 The miR-22-KAT5/CDK8 axis significantly inhibits tumorigenesis of HCC cells. Ectopic expression of Flag-CDK8 or Flag-KAT5 in Huh7 cells transfected with miR-22 mimics significantly attenuated the effects of miR-22 on cell proliferation using MTT assays (A), cell apoptosis (B), transwell cell migration (C), soft agar colony formation (D), and xenograft tumor growth in nude mice (E and F) in which the time course of tumor growth ($n = 10$ mice per group) and representative xenograft tumors at 35 days after inoculation were present.

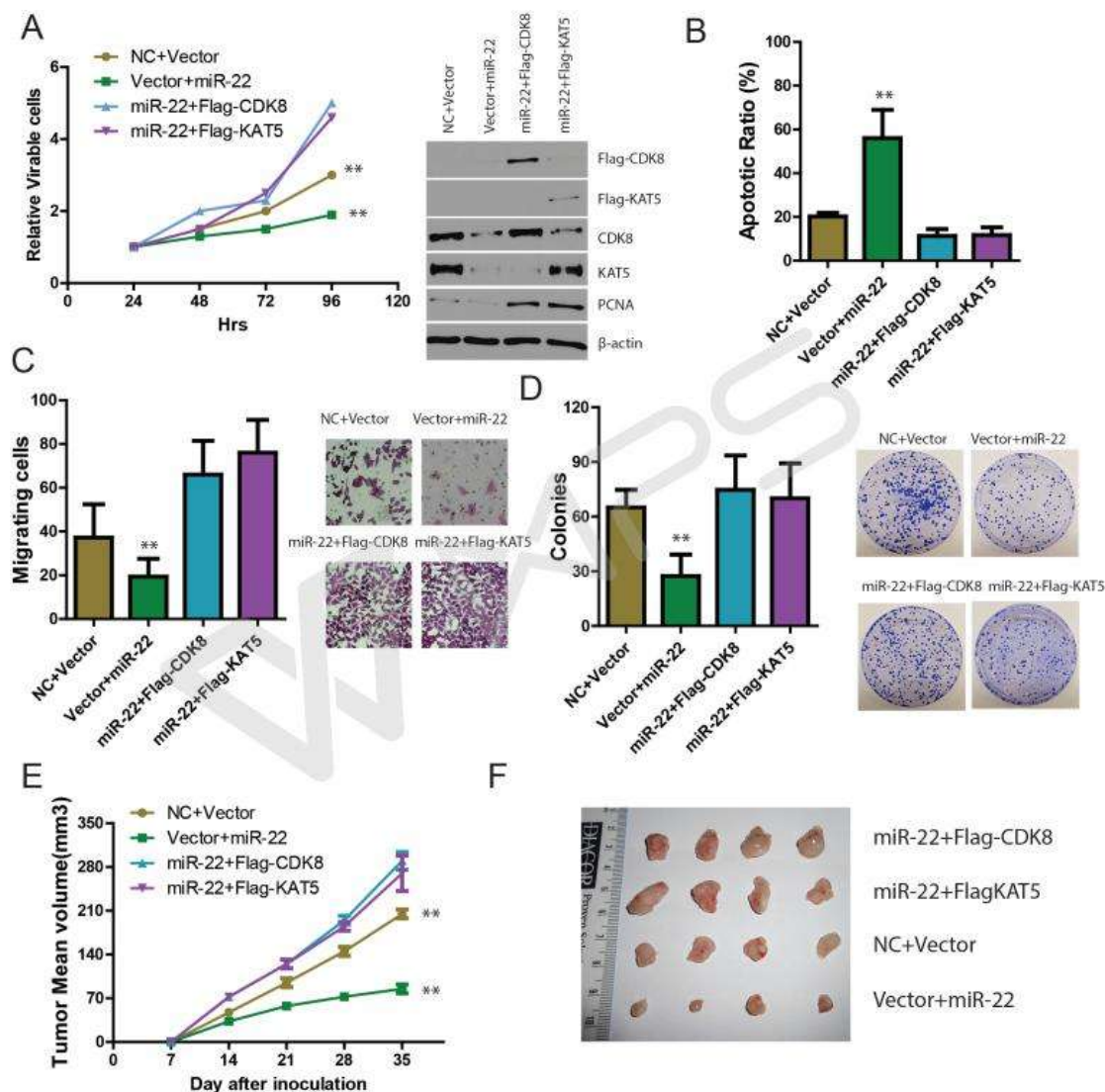


Figure 4 MiR-22 does not decrease the levels of HIF-1 α mRNA and protein, but inhibits HIF-1 α transcriptional activity in HCC cells.

(A) The effect of miR-22 on HIF-1 α mRNA levels in HCC cells. Cells were incubated in the absence or presence of miR-22 for 8 h or 16 h under hypoxic condition. HIF-1 α mRNA levels were measured using qRT-PCR. (B) The effect of miR-22 on HIF-1 α protein levels in HCC cells. HIF-1 α protein levels were detected by immunoblotting, and then protein levels were quantified using Image J software. (C) Inhibitory effect of miR-22 on HIF-1 α transcriptional activity. HCC cells were transiently transfected with the hypoxia-responsive element (HRE) or vascular endothelial growth factor (VEGF)–luciferase vector. Transfected cells were incubated under normoxia or hypoxia in the absence or presence of miR-22 for 24 h. (D) miR-22 suppresses hypoxia-induced HIF-1 α target gene expression. HCC cells were incubated under normoxia or hypoxia in the absence or presence of miR-22 for 24 h. HIF-1 α target gene expression was measured using quantitative RT-PCR. (E) Inhibitory effect of miR-22 on cell migration. HCC cells were seeded into transwell chambers and incubated under normoxia or hypoxia for 24 h in the absence or presence of miR-22. (F) Photograph of tumor samples.

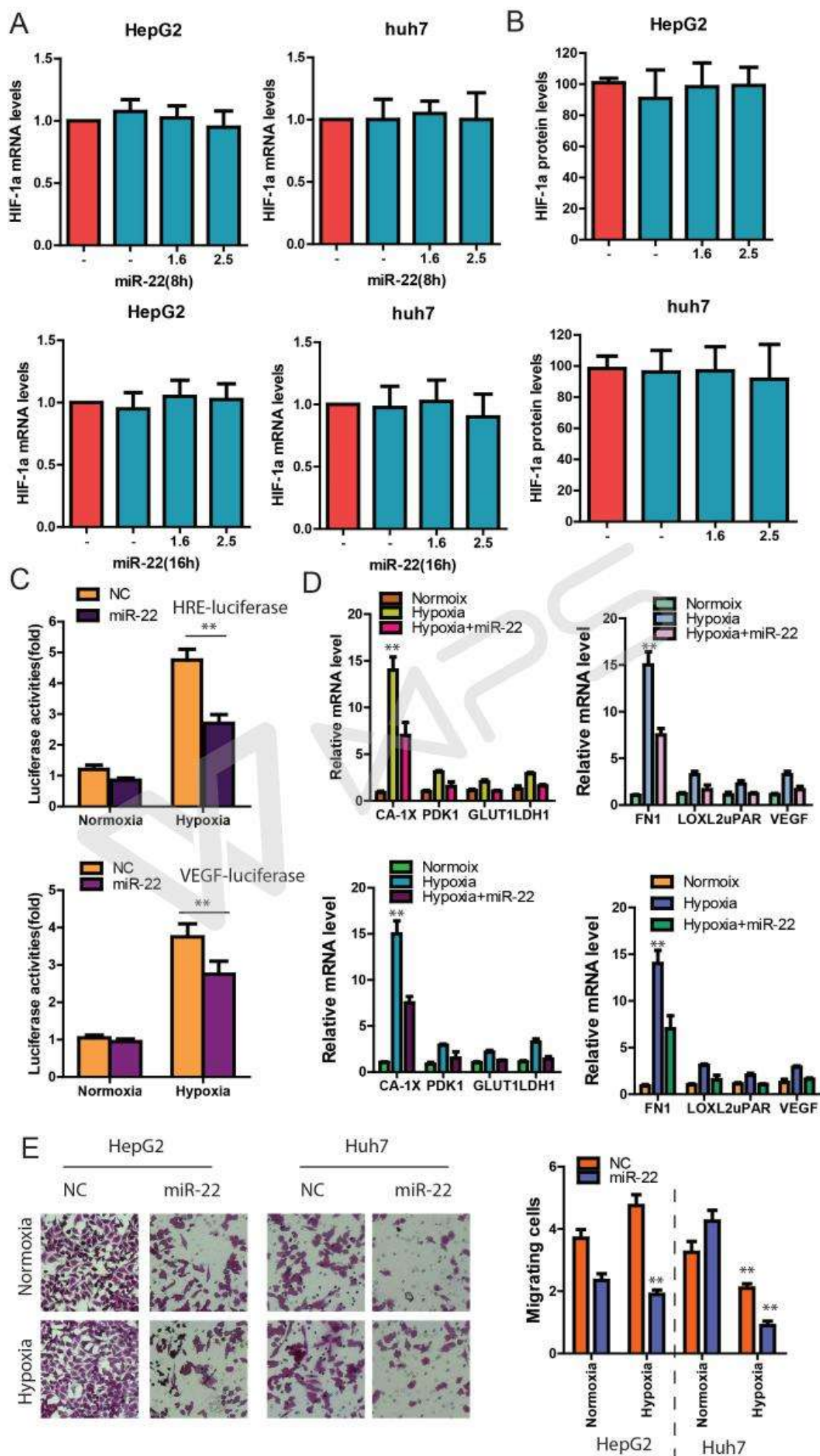


Figure 5 Transcriptional regulation of miR-22 by HIF-1a. (A and B) Huh7 cells were treated with hypoxia (1% O₂) or CoCl₂, respectively. QRT-PCR analysis showed variation of HIF-1a mRNA, and miR-22 levels in HepG2 and Huh7 cultured in 1% O₂ or CoCl₂ for the indicated times. (C) miR-22 expression levels in HepG2 and Huh7 cells transfected with HIF-1a siRNA (siHIF-1a) or negative control (NC) and cultured with or without CoCl₂. D, levels of miR-22 expression in Huh7 cells transfected with HIF-1a overexpression vector (pcDNA-HIF-1a) or empty vector (pcDNA3.1). (E) The HRE sites in human putative *mir-22* promoter proximal region (-1274 to +83 nucleotides for human *mir-22*). (F) After Huh7 cells were cultured in hypoxia or normoxia, CHIP with anti-HIF-1a antibody was performed to verify the binding between HIF-1a and the miR-22 promoter in Huh7 cells. (G) Huh7 cells, which were transfected with empty pGL3 vector (vector) or a miR-22 promoter-containing pGL3 reporter vector (miR-22 promoter), were cotransfected with siHIF-1a or NC. At 24 hours after transfection, the cells were cultured with or without CoCl₂ for 24 hours. Firefly luciferase activity was detected and normalized by Renilla luciferase activity.

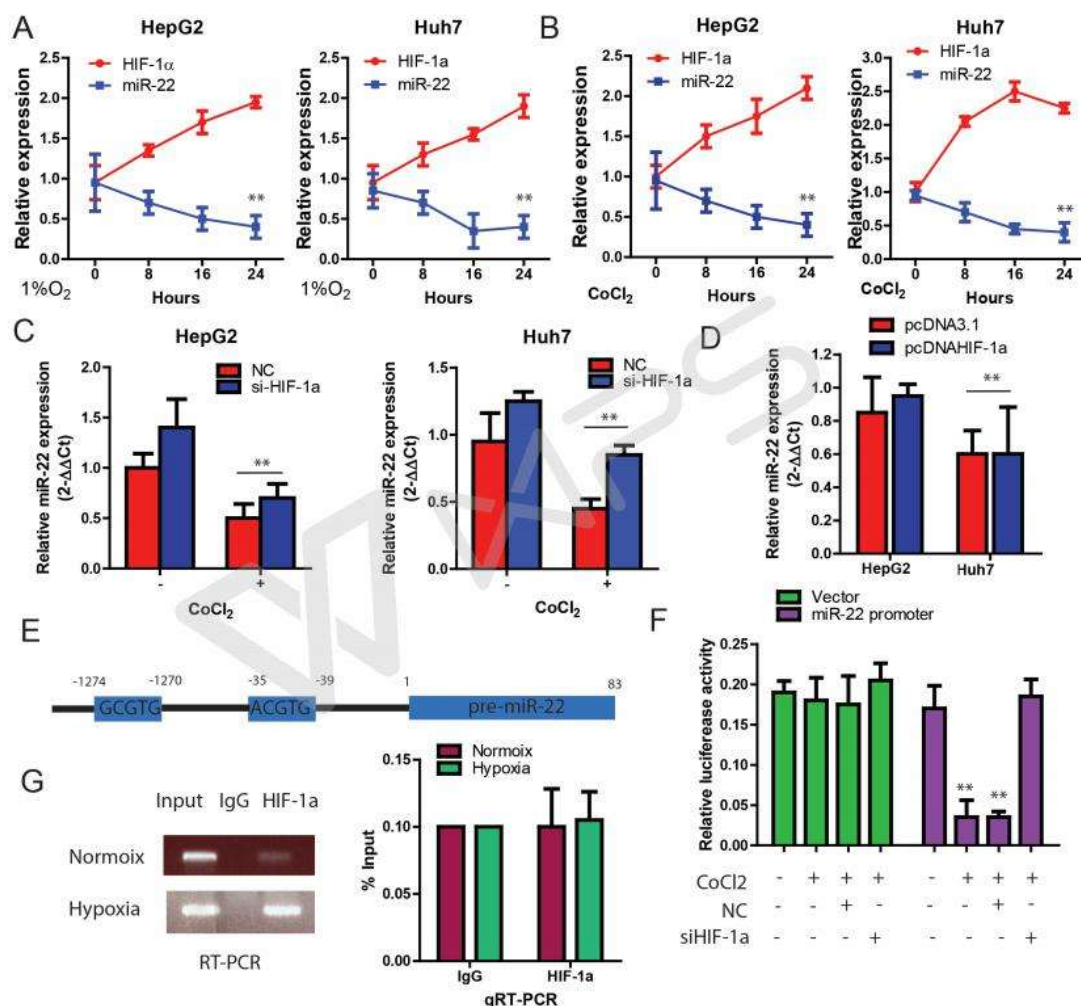


Figure 6 HBx is critical in HBV inhibiting miR-22 expression in HCC cells.

(A) qRT-PCR analysis of miR-22 in HepG2 and HepG2.2.15 cells. (B) qRT-PCR analysis of miR-22 in HepG2 cells transfected with HBV1.3 vector and with the corresponding control. (C) qRT-PCR assay for miR-22 in HBs-, HBc-, HBp-, or HBx-expressing cells and the corresponding controls. The data represent the mean ± SD.

(D) Dual-luciferase assay for the miR-22 promoter activity of HBV or HBx-expressing cells relative to the corresponding control, versus the blank group (n = 5). HBx expression was measured by Western blot (right panel).

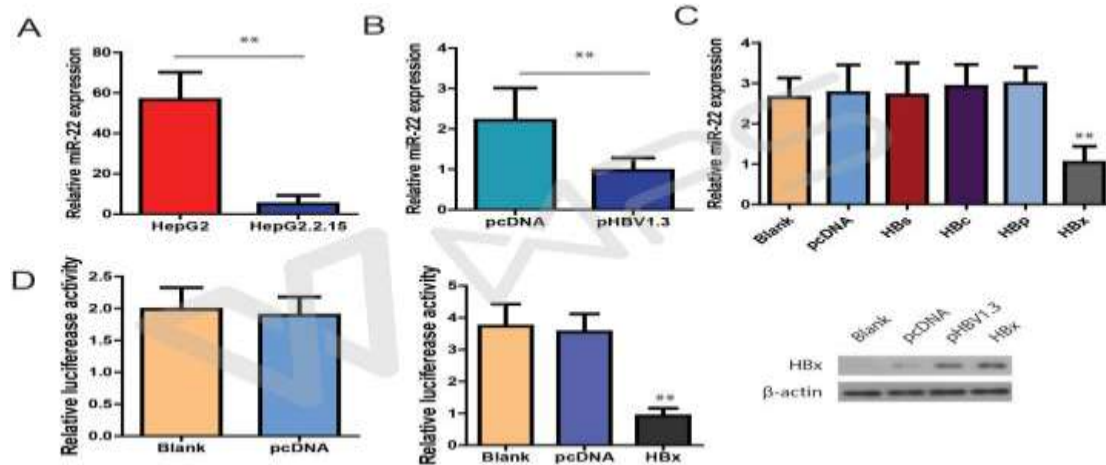


Figure 7 HBx is pivotal in HBV-induced expression of CDK8 and KAT5 protein.

(A) Western blotting analysis for CDK8 and KAT5 in HepG2 and HepG2.2.15 cells. (B) Western blotting analysis for CDK8 and KAT5 in HBs-, HBc-, HBp-, and HBx-expressing HepG2 cells and the corresponding controls and the blank group. (C) Western blotting analysis for CDK8 and KAT5 in HepG2.2.15 cells with HBx inhibition and the corresponding controls respectively.

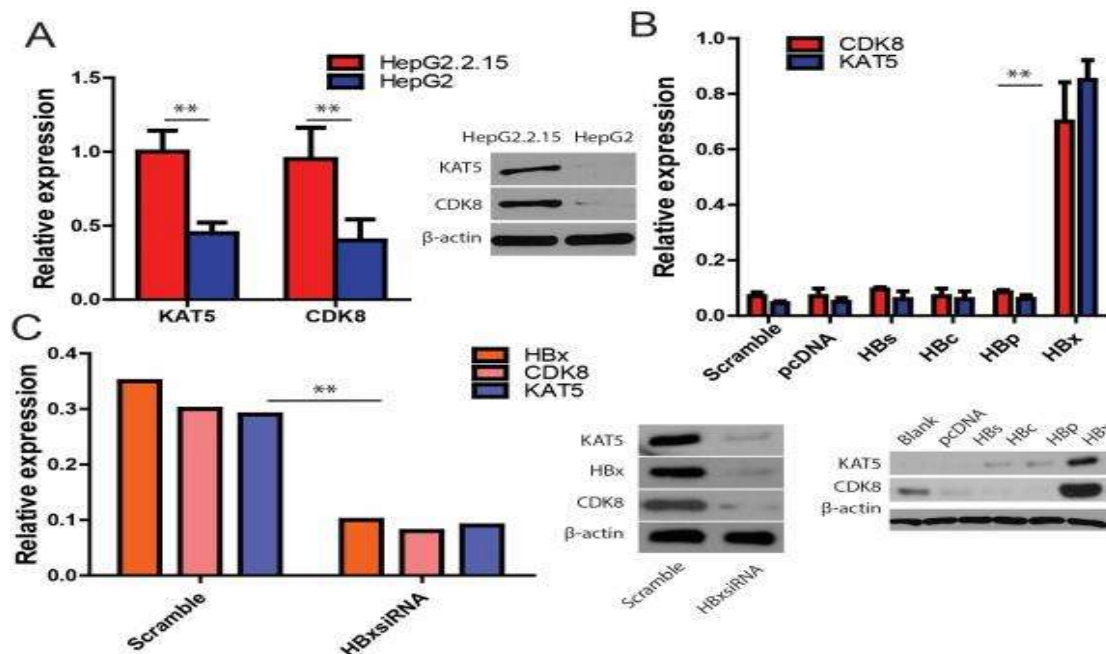
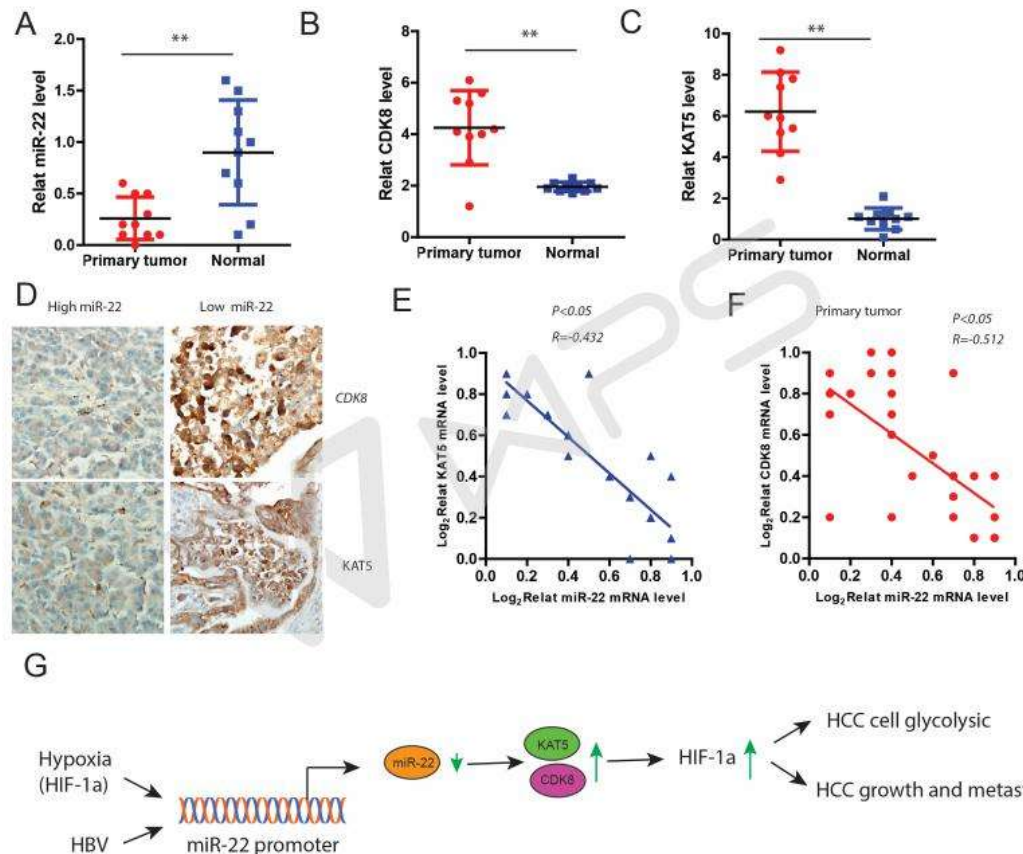


Figure 8 The expression of miR-22, CDK8, and KAT5 is correlated in human HCC specimens. (A–C) The expression of miR-22 (A), *CDK8* (B), and *KAT5* (C) in 60 human HCC and paired normal adjacent tissues. The expression levels of miR-22, *CDK8* and *KAT5* were determined by qRT-PCR. (D) IHC of CDK8 and KAT5 in HCC samples as indicated. (E and F) Pearson's correlation analyses of miR-22 and *CDK8* (E) or *KAT5* mRNA

levels (F) in 60 human HCC specimens. Statistics: Pearson's correlation analyses.(G) Model of miR-22 as a key regulatory node linking hypoxia to deregulated glucose metabolism in HCC.



Discussion

While there is no doubt that insights into the alteration in HCC cells glycolysis will hold promise for potential cancer therapy, the underlying molecular mechanisms remain largely unclear. In the present study, we revealed an unexpected function of miR-22 in inhibiting aerobic glycolysis in HCC cells, aside from the previously reported roles of miR-22 in resistance to HCC therapies and hypoxia (7, 16). The initial observation that miR-22 expression was decreased in HCC cells led us to explore the role of this tumor suppressor in inhibiting Warburg effect. As expected, we verified the correlation between miR-22 expression level and glucose uptake, lactate production, or oxygen consumption rate in HCC cells. Furthermore, silencing miR-22 in HCC

cells increased the aerobic glycolytic phenotype, while cells with forced expression of miR-22 impaired Warburg effect. Mechanistically, miR-22 decreased the activity of HIF1 α protein through directly targeting CDK8 and KAT5, forming a negative feedback loop of HIF1 α /miR-22/CDK8/KAT5/HIF1 α . Interestingly, we also indicated that HBx inhibited the miR-22 while elevated CDK8/KAT5 expression in HCC cells. Thus, these findings reveal a previously unappreciated function of miR-22 in cancer cell metabolism and collectively highlight that miR-22 inhibits glucose metabolism reprogramming through suppressing CDK8/KAT5/HIF1 α axis in HCC. Considering the aberrant expression of miR-22 in various cancer cells and the emerging importance of aerobic glycolysis for cancer development, our findings are potentially

significant for designing new strategies for cancer therapy.

Our findings suggest that miR-22 forms a negative feedback circuit with hypoxia signaling. Previous study indicated that miR-22 directly inhibited the hypoxia signaling in colon cancer (16). Consistent with this previous report, our current results demonstrated that miR-22 decreased the activity of HIF1 α through directly targeting CDK8 and KAT5 in HCC cells. Furthermore, we provided strong evidence that HIF1 α is also negative regulators of miR-22 levels mainly via their direct transcriptional regulation on miR-22 expression. These findings are of considerable interest because accumulating evidence suggests that not only miRNAs can regulate their target genes, but also these target genes may in turn interact with and regulate these specific miRNAs positively or negatively, either at the transcriptional or post-transcriptional level (17). In this study, we established such a relationship between miR-22 and HIF1 α , whereby we identified CDK8 and KAT5 as two new direct targets of miR-22. Therefore, these findings further extend the observations of others and validate the regulatory effects of miR-22 as fine-tuning elements, critical in the homeostasis of genes in response to hypoxia stimulus. Our results not only add insights to understanding the mechanisms of aerobic glycolysis, but also provide additional link between HCC cell metabolism and cancer progression.

Another novel finding of this study was that we identified two conserved HRE within the proximal promoter region of the miR-22 host gene. A reporter gene expression assay indicated that these elements are necessary to inhibit miR-22 promoter activity. These HRE presumably block the activation of miR-22 via HIF1 α transcription factor in response to hypoxia signaling. Our study also indicates that HBx inhibits miR-22 promoter activity. This finding is reminiscent of previous

report that HBx enhances the activity of miR-181a promoter via binding to the CREB site in HCC cells during HBV infection (18). Further studies are needed to determine whether HBx affects the binding of other transcriptional factors on the miR-22 promoter.

In summary, our results provide a significant advance in our current understanding of miR-22 signaling and regulation. Our study suggests two novel mechanisms in which HIF1 α and HBx transcriptionally downregulate miR-22 expression in HCC cells by suppressing the promoter activity of miR-22. In turn, miR-22 decreased the activity of HIF1 α protein through directly targeting CDK8 and KAT5, which blocks metabolic switch from oxidative phosphorylation to aerobic glycolysis in HCC cells. Together, our findings support the possibility that HIF1 α /miR-22/CDK8/KAT5/HIF1 α feedback loop represents a novel biomarker and therapeutic target for HCC.

Materials and Methods

Cell culture, Reagents, and Antibodies

The HCC cell lines, HepG2 (HBV negative), HepG2.2.15 (HBV positive), HEK293T and other HCC cell lines were maintained in Dulbecco's modified Eagle's medium (DMEM, Hyclone) supplemented with 10% fetal bovine serum (FBS, Gibco, USA) containing 100 U/ml penicillin and streptomycin at 37 °C in a humidified atmosphere with 5% CO₂. Antibodies against Anti-HIF1 α , β -tubulin (sc-9104), and β -actin (sc-47778) were purchased from Santa Cruz Biotechnology (Santa Cruz, USA). CDK8 antibody (ab54561) and KAT5 antibody (ab2386) were purchased from Abcam.

Plasmids and transfection

MiR-22 mimics, anti-miR-22, and the negative control, were obtained from RiboBio (China). Lentiviral constructs expressing miR-22 (Lenti-miR microRNA precursor clone collection;

System Biosciences, USA) were packaged using the pPACKH1 lenti-vector Packaging Kit (System Biosciences) in HEK293T cells. The scramble control hairpin pCDH-CMV-MCS-EF1-copGFP was purchased from the same vendor for negative control. The virus particles were harvested 3 days after transfection. HCC cells were infected with recombinant lentivirus-transducing units supplemented with 8 mg/ml Polybrene (Sigma). The stable transfected cells were selected using puromycin and confirmed by qRT-PCR. The plasmids expressing the four proteins of HBV (HBx protein, surface antigen (HBsAg), core protein (HBcAg), and DNA polymerase protein (HBp) were cloned using PCR from pHBV1.3. The pcDNA3.1 (pcDNA) was used as the expression vector. SiRNA targeting HBx mRNAs was designed according to the GenScript siRNA Target Finder (<https://www.genscript.com/sslbin/app/rnai>). These siRNA were subcloned into the pRNAT-U6.1/Neo vector with the U6-RNA promoter between the HindIII and BamHI restriction sites. All the constructs were verified by sequencing.

Colony formation assay

The cells were plated in 6-well plates at 500 per well after transfection. After indicated time, the cells were washed twice with PBS, fixed with methanol and stained with 0.5% crystal violet. The number of colonies was counted under a microscope.

Migration and invasion assays

For the cell migration and invasion assay, cells (1×10^5) in serum-free medium were placed into the upper chamber of a 24-well Transwell Chamber (8 μ m pore size, Corning Costar Corporation, USA) which were uncoated or coated with Matrigel (BD Biosciences, USA) after transfection. The chambers were incubated for indicated time with

culture medium containing 10% FBS added to the lower chamber. Cotton swabs were used to remove the non-invaded cells. Cells which had invaded to the lower surface were fixed, stained and counted using an inverted microscope. All experiments were performed in triplicate.

In vivo animal experiments

Male BALB/C nude mice (4–6 weeks old) were purchased from SJA Laboratory Animal Company of China, which were randomly assigned to experimental groups. For xenograft experiments, 1×10^6 cells were injected subcutaneously into the flank of nude mice ($n = 10$ per group). Tumor size was measured with calipers to estimate volume every 7 days until day 28 after injection. The mice were sacrificed and tumors were collected 28 days later. Tumor volume was calculated as follows: $V = \text{length} \times \text{width}^2 / 2$. For lung metastasis assay, 2×10^6 cells were injected into the tail vein of nude mice ($n = 10$ per group). After 8 weeks, mice were sacrificed and lungs were removed, paraffin embedded and subjected to pathological examination. The number of tumor colonies was determined by using a dissecting microscope. All animal studies were conducted according to protocols approved by the Committee on the Ethics of Experimental Animal of Jilin University.

Dual-luciferase reporter assay

A dual-luciferase reporter vector was used to generate the luciferase constructs. To validate whether CDK8 and KAT5 are direct targets of miR-22, wild-type or mutant 3'-UTR of CDK8 and KAT5 were cloned into the pscheck-2 vector (Promega, USA). HEK293T cells were co-transfected with miR-22 mimics or controls and wild-type or mutant 3'-UTR-luc by using Lipofectamine 2000. To validate the HIF1 α -binding sites in the miR-22 promoter, the miR-22 promoter region (–1344/+55 bp, as was described previously)

was amplified from human genomic DNA to generate miR-22 promoter using specific primers. The PCR product was cloned into the pGL3-basic vector (Promega). HCC cells were transfected with pGL3-miR-22 along with pcDNA3.1-HRE expression vector or an empty vector using Lipofectamine 2000. The mutant type in the putative HIF1 α -binding site in the wild-type fragment was also PCR- amplified. The wild-type and mutant reporter constructs along with pcDNA3.1-HIF1 α expression vector or an empty vector were cotransfected into HCC and HEK293T cells. Or hypoxia-responsive element (HRE) promoter-luciferase reporter plasmid was from Addgene plasmid # 26731). After incubation, luciferase activity was measured using a luminometer (Berthold Technologies,Germany) and normalized against β -gal activities to account for transfection efficiency. Or after transfection for 48 h, cells were harvested and assayed with Dual-Luciferase Reporter Assay System (Promega) according to the manufacturer's protocols. Luciferase activity was measured using Dual-Luciferase Reporter Assay Kit (E1960; Promega) on a GLOmax microplate luminometer (Promega). Firefly luciferase signals were normalized using Renilla luciferase signals. All experiments were performed in triplicate.

MTT assay

Indicated cells were seeded into 96-well plates as 2000 cell/well with triplicate and incubated at 37 °C, 5% CO₂ for 24 h. The plasmids were then transfected into cells. After 6 h from transfection, the growth medium was changed. And the cells were continued to be incubated for 48 h and treated using 20 μ l MTT reagent (5 mg/ml) per well. Then the cells were incubated for 4 h until purple precipitate was visible. Culture medium was discarded. Each well was added 150 μ l DMSO and was followed by 10 min oscillation. The absorbance in each well, including the blanks was

measured at 570 nm in a multimode plate reader (EnSight™). The relative OD values of experimental group versus the blank group were recorded.

Cell viability assay

To determine the cell viability, the cells were fixed with 4% paraformaldehyde for 15 min and stained with 0.05% crystal violet staining solution (HT90132, Sigma-Aldrich) for 15 min. To measure optical density, the cells were treated using 1% sodium dodecyl sulfate (SDS) solution for 15 min at room temperature. The dissolved solutions were transferred to a 96-well plate and samples were measured at 595 nm using a microplate reader (BioTek, USA).

Measurement of glucose uptake and lactate production

According to the manufacturer's protocols, glucose (HK) assay reagent kit (GAHK20, Sigma) and lactate assay kit (K627-100, BioVision) were respectively used to measure the concentration of D-glucose and lactate in cell culture supernatants and sample tissues. Values were normalized to cell number or tissue mass.

Western blotting

Total proteins were extracted using cell lysis buffer (1% NP-40, 150 mM NaCl, 50 mM Tris pH 7.4, 2 mM EDTA, and protease inhibitor cocktail). Cell lysates were separated by 7.5% or 10% SDS-polyacrylamide gel electrophoresis (PAGE). Separated proteins were transferred onto an Immobilon-P membrane (Millipore, USA). The transferred membranes were blocked with 5% skim milk in Tris-buffered saline containing 0.05% Tween-20 (TBS-T) for 1 h at room temperature, and then incubated with indicated primary antibodies diluted at 1:1000 or 1:5000 in 5% skim

milk in TBS-T at 4 °C overnight. Horseradish peroxidase-conjugated secondary antibodies were incubated for 1 h at room temperature. Proteins were detected using the enhanced chemiluminescence kit (Pierce) and bands quantified with Science Lab 2003 Image Gauge (Fujifilm, Japan).

Immunohistochemistry

Tumor tissues extracted from human and mice tissues were fixed with paraformaldehyde for HE and immunohistochemical staining. After neutralization of endogenous peroxidase was performed, slides were blocked with 5 % bovine serum albumin for 1 h and incubated with specific primary antibodies overnight at 4 °C, which was followed by incubation with HRP-labelled anti-rabbit secondary antibody for 1 h at room temperature. Visualisation was performed using 3, 30-diaminobenzidine tetra- hydrochloride and counterstained with haematoxylin.

Cell proliferation assay

Cell Counting Kit-8 (CCK-8) was used to determine cell numbers according to the manufacturer's instructions. Briefly, 2×10^3 cells were seeded into 96-well plates containing 100 μ l complete medium. At the indicated time, 20 μ l CCK-8 was added to each well and incubated at 37°C. The absorbance was measured at 450 nm wavelength using a plate reader after an hour.

Quantitative Real-Time PCR

Total RNA was isolated from different cell lines and liver tissues using TRIzol reagent following the manufacturer's instructions (Life Technologies). And 2 μ g of this RNA was used to synthesize cDNA using Superscript-III Reverse Transcriptase (Life Technologies) and quantified using SYBR Green PCR Master Mix (Roche Diagnostics) and

gene-specific primers in QuantStudio 7 Flex RealTime PCR system (Thermo Fisher Scientific, USA). MicroRNA was quantified using TaqMan miRNA Assay kit (Life Technologies). The sequences of the PCR primers (5'-3') were: GACAGCCTCACAAACAGAG and CTCAAAGCGACAGATAACACG for HIF1 α ; CCACTCCAGCAGGGAAGG and GCGACGCAGCCTTTGAAT for CA-IX; ATGGAGCCCAGCAGCAA and GGCATTGATGACTCCAGTGTT for GLUT1; CTACCTCCACCATGCCAAGT and AGCTGCGCTGATAGACATCC for VEGF; TGAACATTCTGGCTGGTGACAGGA and ATGATGTCATTCCCACAATGGCCC for PDK1; CACTGCGGATCCCTGAAAC and CCTGTCTTCGGGCTGATG for LOXL2; CCATAAAGGGCAACCAAGAG and ACCTCGGTGTTGTAAGGTGG for FNI; AGCCTTACCGAGGTTGTGTG and AAATGCATTTCGAGGTAACGG for uPAR. For β -actin: CCAACTGGGACGACAT and AGCCTGGATAGCAACG; HBx: TCTGTGCCTTCTCATCTGC and TCGGTGCTTGACATTGCTG; miR-22: ACACTCCAGCTGGGAAGCTGCCAGTTGAAG and GGTGTCGTGGAGTCGGCAA; the primers for U6 were: CGCTTCGGCAGCACATATAC and TTCACGAATTTGCGTGTCAT. The relative expression of miRNA or mRNA was analyzed using the $\Delta\Delta$ Ct method. Δ Ct was calculated by subtracting the Ct of U6 (for miRNA) or β -actin (for mRNA) RNA from the Ct of the miRNA or mRNA of interest. The $\Delta\Delta$ Ct was calculated by subtracting the Δ Ct of the reference sample from the Δ Ct of each sample. The fold change was determined using the equation $2^{-\Delta\Delta$ Ct}.

Chromatin immunoprecipitation (ChIP) assay

ChIP assays were performed as described previously (19). Cells with different treatment were fixed with 1% formaldehyde to cross-link

chromatin and proteins for 15 min at room temperature, and terminated by a final concentration of 0.125 M glycine. Then cells were lysed using 300µl lysis buffer (50 mM Tris-HCl, pH 8.0, 150 mM NaCl, 5 mM EDTA, 1% Nonidet P-40, 0.5% deoxycholate, and protease inhibitors). The cell lysates were sonicated in ice water bath to yield chromatin fragments about 600 bp. After centrifugation at 13,000 rpm for 10 min, the supernatants were pre-cleared for 15 min at 4°C via with 30µl of protein A-Sepharose beads. Then the supernatants were divided into three equal parts: one for input, the other two for immunoprecipitation with or without HIF1α antibody. 24 hours later, the immune complexes were precipitated with protein A-Sepharose beads, then the beads were collected after washed twice with the wash buffer I (20 mM Tris-HCl, pH 8.1, 150 mM NaCl, 0.1% SDS, 1% Triton X-100, and 2 mM EDTA), followed by wash buffer II (20 mM Tris-HCl, pH 8.1, 500 mM NaCl, 0.1% SDS, 1% Triton X-100, and 2 mM EDTA), and wash buffer III (10 mM Tris-HCl, pH 8.1, 0.25 M LiCl, 1% Nonidet P-40, 1% deoxycholate, and 1 mM EDTA), and the final wash buffer IV (10 mM Tris-HCl, pH 8.1, and 1 mM EDTA). The immunoprecipitates were eluted by 200µl elution buffer (1% SDS and 0.1 M NaHCO₃), followed by incubation at 65°C overnight. The next day, DNA of each sample was isolated, and PCR was performed to amplify the promoter segments containing a HIF1α binding site. The sequences of PCR primers for the quantitative ChIP assay (5'–3') are ATCTGAGCAACGAGACCAAA and CACGTGCTCGTCTGTGTTTA.

Measurement of cellular respiration and extracellular acidification (bioenergetic profile)

The XF24 extracellular flux analyzer (Seahorse Biosciences, USA) was used to determine the bioenergetic profile of intact cells. The extracellular acidification rate (ECAR) was

recorded to assess the mitochondrial respiratory activity and glycolytic activity, respectively. After four measurements under basal conditions, cells were treated sequentially with 1 uM oligomycin, 0.6 uM carbonyl cyanide *p*-(trifluoromethoxy)phenylhydrazone (FCCP), 0.4 uM FCCP, and 0.5 uM rotenone plus 0.5 uM antimycin A (Sigma-Aldrich), with three consecutive determinations under each condition that were subsequently averaged. ATP turnover was estimated from the difference between the basal and the oligomycin-inhibited respiration, and the maximal respiratory capacity was the rate in the presence of the uncoupler FCCP. Nine independent replicas of each analysis were done, and results were normalized according to protein concentrations.

Clinical specimens

This study was approved by the ethic committee of Jilin University. Clinical specimens were collected after the consent of the patients. The cancer tissues were kept at –80 °C.

Statistical Analysis

Statistical analyses were performed using SPSS 17.0 software (SPSS Inc., USA). All data were analyzed using an unpaired Student's *t*-test for two experimental comparisons and a one-way ANOVA (analysis of variance) followed by Tukey's post hoc test for multiple comparisons using GraphPad Prism 5.01 (GraphPad Software Inc., USA). Gene expression correlation was calculated by Pearson's chi-squared test. Data are represented as means ± standard deviations (SDs). Statistically significant difference was defined as $P < 0.05$.

Abbreviations

HCC: hepatocellular carcinoma; miR: microRNAs; 3'-UTR: 3'- untranslated regions; GAPDH:

glyceraldehyde-3-phosphate dehydrogenase; PBS: phosphate-buffered saline; RT-PCR: reverse transcription-polymerase chain reaction; HIF1 α : Hypoxia-inducible factor α ; ANOVA: analysis of variance; ChIP: Chromatin immunoprecipitation.

CONFLICTS OF INTEREST

The authors declare no conflicts of interest.

GRANT SUPPORT

This study was supported by grant from Jilin University (JDYY82017001)

This work was supported by National Natural Science Foundation of China 31571241, 31660266(H Huang), Teacher Research Foundation of Central South University 2013jsjj036 (H Huang)

References

- [1]. Qu C, He D, Lu X, Dong L, Zhu Y, Zhao Q, Jiang X, Chang P, Jiang X, Wang L, Zhang Y, Bi L, He J, Peng Y, Su J, Zhang H, et al. Salt-inducible Kinase (SIK1) regulates HCC progression and WNT/beta-catenin activation. *Journal of hepatology*. 2016; 64(5):1076-1089.
- [2]. Zhang H, Guo X, Feng X, Wang T, Hu Z, Que X, Tian Q, Zhu T, Guo G, Huang W, Li X. MiRNA-543 promotes osteosarcoma cell proliferation and glycolysis by partially suppressing PRMT9 and stabilizing HIF-1 α protein. *Oncotarget*. 2017 Jan 10;8(2):2342-2355.
- [3]. Song R1, Song H, Liang Y, Yin D, Zhang H, Zheng T, Wang J, Lu Z, Song X, Pei T, Qin Y, Li Y, Xie C, Sun B, Shi H, Li S, Meng X, Yang G, Pan S, Zhu J, Qi S, Jiang H, Zhang Z, Liu L. Reciprocal activation between ATPase inhibitory factor 1 and NF- κ B drives hepatocellular carcinoma angiogenesis and metastasis. *Hepatology*. 2014 Nov;60(5):1659-73.
- [4]. He D, Huang C, Zhou Q, Liu D, Xiong L, Xiang H, Ma G, Zhang Z. HnRNP K/miR-223/FBXW7 feedback cascade promotes pancreatic cancer cell growth and invasion. *Oncotarget*. 2017 Mar 21;8(12):20165-20178
- [5]. Shen J, Wang Q, Gurchich I, Remotti H, Santella RM. Evaluating normalization approaches for the better identification of aberrant microRNAs associated with hepatocellular carcinoma. *Hepatology Res*. 2016 Nov;2:305-315.
- [6]. Ma F, Song H, Guo B, Zhang Y, Zheng Y, Lin C, Wu Y, Guan G, Sha R, Zhou Q, Wang D, Zhou X, Li J, Qiu X. MiR-361-5p inhibits colorectal and gastric cancer growth and metastasis by targeting staphylococcal nuclease domain containing-1. *Oncotarget*. 2015 Jul 10;6(19):17404-16.
- [7]. Zhang J, Yang Y, Yang T, Liu Y, Li A, Fu S, Wu M, Pan Z, Zhou W. microRNA-22, downregulated in hepatocellular carcinoma and correlated with prognosis, suppresses cell proliferation and tumorigenicity. *Br J Cancer*. 2010 Oct 12;103(8):1215-20.
- [8]. Zhou L, He J, Zhang Y. MicroRNA-22 expression in hepatocellular carcinoma and its correlation with ezrin protein. *J Int Med Res*. 2013 Aug;41(4):1009-16.
- [9]. Joel I. Perez-Perri, Veronica L. Dengler, K. Audrey Audetat, Ahwan Pandey, Elizabeth A. Bonner Marjeta Urh, Jacqui Mendez, Danette L. Daniels, Pablo Wappner, Matthew D. Galbraith, 2,3,* and Joaquín M. Espinosa. Cell Rep. The TIP60 complex is a conserved coactivator of HIF1A. *Cell Rep*. 2016 Jun 28; 16(1): 37-47.
- [10]. Chanmee T, Ontong P, Izumikawa T, Higashide M, Mochizuki N, Chokchaitaweek C, Khansai M, Nakajima K, Kakizaki I, Kongtawelert P, Taniguchi N, Itano N. Hyaluronan Production Regulates Metabolic and Cancer Stem-like Properties of Breast Cancer Cells via Hexosamine Biosynthetic Pathway-coupled HIF-1 Signaling. *J Biol*

- Chem. 2016 Nov 11;291(46):24105-24120.
- [11]. Paolicchi E, Gemignani F, Krstic-Demonacos M, Dedhar S, Mutti L, Landi S. Targeting hypoxic response for cancer therapy. *Oncotarget*. 2016 Mar 22;7(12):13464-78.
- [12]. Fukushima S, Endo M, Matsumoto Y, Fukushi JI, Matsunobu T, Kawaguchi KI, Setsu N, Iida K, Yokoyama N, Nakagawa M, Yahiro K, Oda Y, Iwamoto Y, Nakashima Y. Hypoxia-inducible factor 1 alpha is a poor prognostic factor and potential therapeutic target in malignant peripheral nerve sheath tumor. *PLoS One*. 2017 May 30;12(5):e0178064.
- [13]. Ikeda S, Kitadate A, Abe F, Saitoh H, Michishita Y, Hatano Y, Kawabata Y, Kitabayashi A, Teshima K, Kume M, Takahashi N, Tagawa H. Hypoxia-inducible microRNA-210 regulates the DIMT1-IRF4 oncogenic axis in multiple myeloma. *Cancer Sci*. 2017 Apr;108(4):641-652.
- [14]. Long JI, Badal SS, Wang Y, Chang BH, Rodriguez A, Danesh FR. MicroRNA-22 is a master regulator of bone morphogenetic protein-7/6 homeostasis in the kidney. *J Biol Chem*. 2013 Dec 20;288(51):36202-14.
- [15]. Wang X, Oishi N, Shimakami T, Yamashita T, Honda M, Murakami S, Kaneko S. Hepatitis B virus X protein induces hepatic stem cell-like features in hepatocellular carcinoma by activating KDM5B. *World J Gastroenterol*. 2017 May 14;23(18):3252-3261
- [16]. Yamakuchi M, Yagi S, Ito T, Lowenstein CJ. MicroRNA-22 regulates hypoxia signaling in colon cancer cells. *PLoS One*. 2011;6(5):e20291
- [17]. Natalia J. Martinez and Albertha J. M. Walhout. The interplay between transcription factors and microRNAs in genome-scale regulatory networks. *Bioessays*. 2009 Apr; 31(4): 435-445.
- [18]. Yi Tian, Xinqiang Xiao, Xing Gong, Feng Peng, Yun Xu, Yongfang Jiang, and Guozhong Gong. HBx promotes cell proliferation by disturbing the cross-talk between miR-181a and PTEN. *Sci Rep*. 2017; 7: 40089. Published online 2017 Jan 5.
- [19]. Gao X, Hicks KC, Neumann P, Patel TB. Hypoxia inducible factors regulate the transcription of the sprouty2 gene and expression of the sprouty2 protein. *PLoS One*. 2017 Feb 14;12(2):e0171616.